Kinetic modelling along with gas flow simulation of N_2-O_2 plasma afterglows in a plasma-chemical reactor

A. Annušová[1,2], C. Foissac[1], P. Veis[2] and P. Supiot[1]

[1]*Institute of Electronics, Microelectronics and Nanotechnology (IEMN) UMR-CNRS 8520, Lille 1 University, 59650 Villeneuve d'Ascq, France*
[2]*Department of Experimental Physics, Faculty of Mathematics, Physics and Informatics, Comenius University, Mlynská dolina F2, 84248 Bratislava, Slovakia*

We hereby present the characterisation of the late afterglow of a N_2-O_2 microwave plasma, by interrelated kinetic modelling based on experimental results obtained by optical emission spectroscopy and mass spectrometry, and reactive gas flow simulation performed with COMSOL Multiphysics®. The discharge is excited at 433 MHz at pressure of 440 Pa. The afterglow flows to the plasma processing chamber of the reactor. The results of 0D modelling and reactive flow simulation show good consistency with each other and point out the main mechanisms in the studied media simplifying kinetic schemes for future use.

1. Introduction

N_2-O_2 mixtures discharges are important for industrial purposes but also fundamental research [1]. So far their interesting and complex kinetic scheme encouraged a lot of theoretical and experimental investigations [2, 3]. However there is still a lack for research involving modelling studies that are supported by experimental results for confirmation and adjusting of calculations. We have implemented this type of simultaneous study but with an original approach on O_2 injection either upstream or downstream of the discharge creating a N_2-O_2 plasma and a N_2-O_2 afterglow of a N_2 plasma, respectively. We show that the completion of this kinetic modelling with gas flow simulation can be a very effective way to account for the plasma properties as also to indicate clearly the main mechanisms leading to define the species production and destruction.

2. Experimental section

2.1. Experimental set-up

The Fig. 1 presents the schema of the experimental set-up and the illustration of the gas velocity field simulated in COMSOL Multiphysics® at a gas temperature of T_g = 300 K.

The mounting constitutes of a microwave cavity excited at 433 MHz with a power value fixed at 250 W, a discharge tube, a stainless steel plasma-chemical reactor covered with aluminium thin sheet, a symmetrical pumping system and the diagnostic tools (mass and optical emission spectrometers). The working pressure is 440 Pa. The installation of the mass spectrometer required differential pressure pumping (values indicated in Fig. 1). The N_2 flow rate was fixed at 1500 sccm while O_2 with flow rate, Q(O_2), up to 500 sccm (25 %) was injected either upstream of the discharge (D) together with N_2 or through a stainless steel injector placed in the reactor. The latter means the injection of O_2 directly in the Lewis-Rayleigh Afterglow (LRA) region.

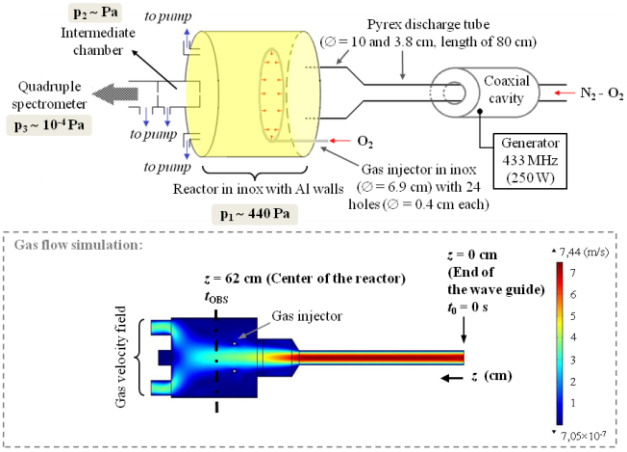

Fig. 1: Experimental set-up.

The simulation of the laminar flow enables to define the observational points of the plasma through time, *t* (details in [4]). On this basis we have calculated for our conditions (T_g = 400 K determined from optical emission spectroscopy) the characteristic time corresponding to the centre of the reactor (*z* = 62 cm) to be t_{OBS} = 152 ms.

2.2. Diagnostic techniques and data exploitation

Optical emission spectroscopy was used to study principally the LRA by recording at t_{OBS} = 152 ms the emission from the first positive system (1PS) of N_2, NO_β system and in the case of O_2 injection into the D also the continuum emission denoted NO_2*, i.e. $N_2(B^3\Pi_g \rightarrow A^3\Sigma_u^+)$, $NO(B^2\Pi \rightarrow X^2\Pi)$ and

$NO_2(A^2B_2 \rightarrow X^2A_1)$ transitions, respectively. The D was also monitored due to some problems with parasitic emission detected in the LRA. The study of the vibrational distribution of the 1PS and applying the abacus method (introduced by Mérel *et al.* [5]) helped to overcome this problem and differentiate the two signals (details in [4]). It is well known, that the collision of two $N(^4S)$ atoms and a N_2 molecule is the main mechanism to populate $N_2(B^3\Pi_g)$ in the LRA and is a resonant process for the vibrational level v =11. So the concentration of this specie is proportional to the square of the concentration of $N(^4S)$ atoms which allowed us to obtain their relative densities. Spectrometers Jobin Yvon HR 460 ($\Delta\lambda$ = 0.2 nm at 770 nm) and Ocean Optics HR4000CG ($\Delta\lambda$ = 0.75 nm at 546 nm) were used to study the LRA and D, respectively.

According to the used setup, the quadruple mass spectrometer (model Pfeiffer QME 200 with channeltron, mass resolution: $\Delta m/m$ = 0.02) allowed the species detection only in the LRA. We were interested in the concentration of $N(^4S)$ atoms. As the signal belonging to the atoms formed by ionization is carrying this information, we have scanned the signal from the LRA with and without ignited plasma to dispose of the signal coming from dissociative ionization of N_2 molecules in the chamber of the spectrometer.

3. Kinetic modelling

On the basis of the experimental results we have built a 0D temporal model as function of the point and quantity of O_2 injected, in order to account for the density variations of N_2, $N(^4S)$, O_2, $O(^3P)$, $NO(X^2\Pi)$, $NO_2(X^2A_1)$ and O_3 species. The steady kinetic relations of the $NO(B^2\Pi)$ and $NO_2(A^2B_2)$ emitters also allowed to account for their relative concentrations. The complete reaction scheme is a simplified one. It is described in detail in our previous work with a complete set of results [4, 6].

The Fig. 2 shows the comparison of results from calculation with experiment for $N(^4S)$, $NO(B^2\Pi)$ and $NO_2(A^2B_2)$ states for the two cases of O_2 injection. The experimental relative densities are normalized to the ones from the calculation. The obtained results from both diagnostic techniques on the $N(^4S)$ density variation are identical. It is important to note that in the case of O_2 injection in the D, a characteristic flow rate value exists at which the $N(^4S)$ and $NO(B^2\Pi)$ species disappear but the NO_2* continuum begin to increase sharply. This evidences an important connection between these species and $O(^3P)$ atoms that governs the kinetic of the media [4]. The case of O_2 injection in the LRA shows different trends. Moreover, the $NO_2(A^2B_2)$ state was not observed in this case. We can state that two different kinetic schemes can be considered, but the strong relation between the mentioned species remains [4]. This can be very interesting for deposition processes, for instance, when assuming N_2-O_2 mixtures as the different point of injection change the production rates of active species which can then influence the properties of the prepared films.

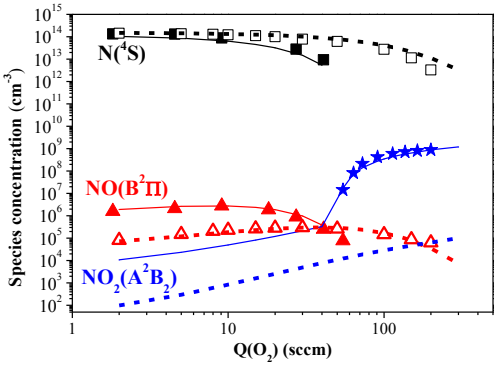

Fig. 2: Species densities obtained from the model (lines) compared to the experimental results (symbols). The full or dashed lines, as well as the full or empty symbols, illustrate the case of O_2 injected in the D or LRA, respectively.

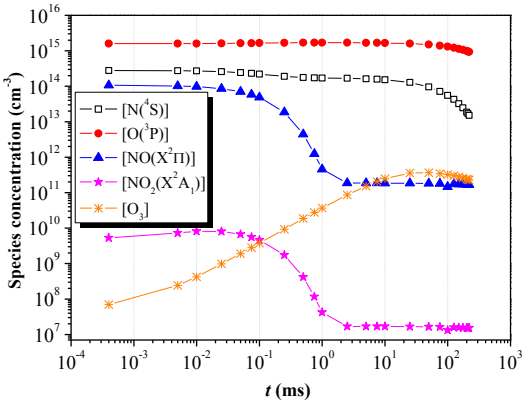

Fig. 3: Temporal evolution of species densities at 20 sccm O_2 injected in D.

The Fig. 3 presents an example of the species density temporal evolution at $Q(O_2)$ = 20 sccm injected in D. We can observe a coherent evolution of $NO(X^2\Pi)$ and $NO_2(X^2A_1)$ with time, pointing out again the existence of a simple relation between them. This figure also shows how the $N(^4S)$ atoms become progressively converted to NO molecules and then with $O(^3P)$ atoms to $NO_2(X^2A_1)$ in the reactor (i.e. around 150 ms). Ozone is produced constantly during the flow.

4. Gas flow simulation and comparison with modelling results

The Tab. 1 presents the simplified kinetic scheme based on the 0D model that has been introduced into the COMSOL software [4], together with the reactors geometry to account for the temporal evolution of densities of the main species displayed in a 2D figure. Reactions for radiative and collisional quenching of $NO(B^2\Pi)$ and $NO_2(A^2B_2)$ species are not shown but taken into account. The software solves the system of coupled equations of conservation of densities while the implemented initial values results from the kinetic model at the specified mixture composition.

Tab. 1: Reactions introduced in COMSOL Multiphysics® reactive flow simulation

Reactions	N°
$N(^4S) + O_2(X^3\Sigma_g^-) \rightarrow NO(X^2\Pi) + O(^3P)$	(1)
$N(^4S) + O(^3P) + N_2 \rightarrow NO(X^2\Pi) + N_2$	(2)
$N(^4S) + NO(X^2\Pi) \rightarrow N_2(X^1\Sigma_g^+, v = 3) + O(^3P)$	(3)
$N(^4S) + surface \rightarrow$ products	(4)
$N(^4S)(surface) + O(^3P)(surface) + wall \rightarrow NO(X^2\Pi)$	(5)
$O(^3P) + O(^3P) + N_2 \rightarrow O_2(X^3\Sigma_g^-) + N_2$	(6)
$O(^3P) + O_2(X^3\Sigma_g^-) + N_2 \rightarrow O_3 + N_2$	(7)
$O(^3P) + O_3 \rightarrow 2\ O_2(X^3\Sigma_g^-, a\ ^1\Delta_g)$	(8)
$O(^3P) + surface \rightarrow O(^3P)(surface)$	(9)
$N(^4S) + O(^3P) + N_2 \rightarrow NO(B^2\Pi) + N_2$	(10)
$O(^3P) + NO(X^2\Pi) + N_2 \rightarrow NO_2(A^2B_2) + N_2$	(11)

The figures 4 and 5 present the results of the flow simulation for the densities of the main species in their ground and excited states, respectively, with the help of a surface colour code, for the condition $Q(O_2)$ = 30 sccm (injected in D) close to that considered in the 0D model.

In general terms we can state that the results are in a very satisfying agreement with the temporal model. Nitrogen atoms (Fig. 4 (a)) are rapidly destructed in the first afterglow instants then a slower trend appears until they reach the reactor. We observe a decrease by a factor of 3 - 4 between the entrance and the centre of the reactor at the characteristic t_{OBS} = 152 ms, which coincides with the 0D model results. The $O(^3P)$ atoms (Fig. 4 (b)) undergoes relatively small changes on the axis, but shows very marked variations nearby the walls in the late afterglow processing reactor chamber. The $NO(X^2\Pi)$ density (Fig. 4 (c)) is relatively low and steady after a very sharp fall immediately after the entry of the mixture into the tube [6]. This result

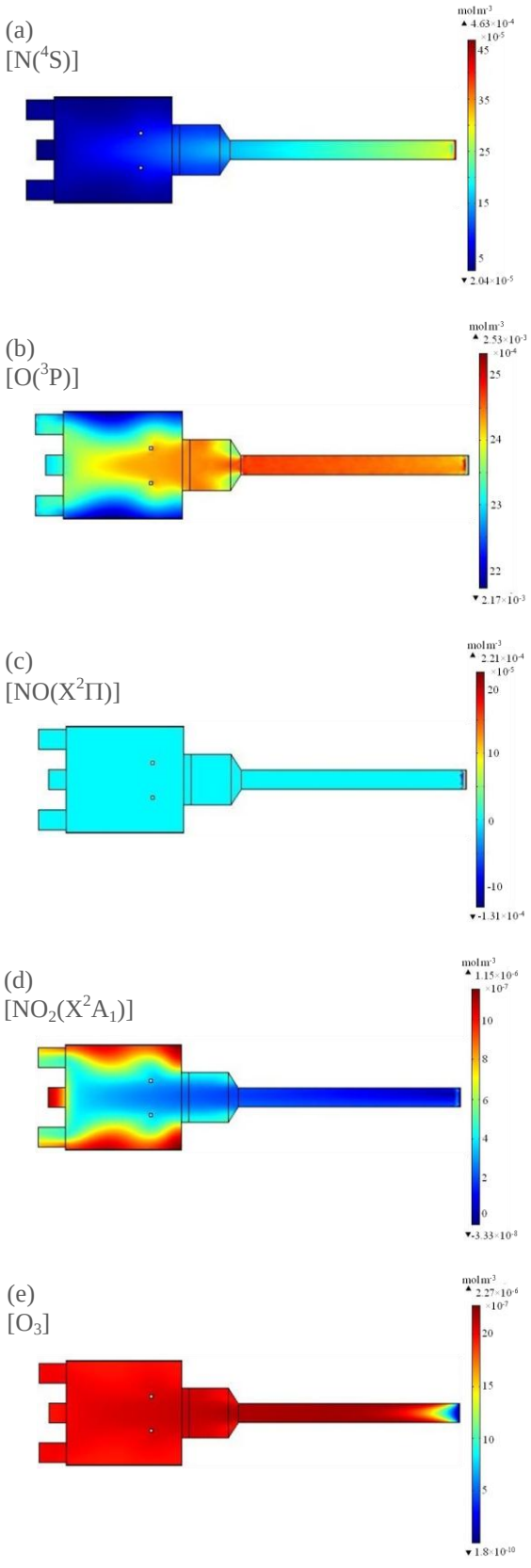

Fig. 4: COMSOL Multiphysics® simulation of the reactive flow of species in ground states at $Q(O_2)$ = 30 sccm (injected in D). Same configuration as in speed field shown in Fig. 1. The species densities are expressed in $mol.m^{-3}$.

qualitatively reproduces the results obtained from the 0D simulation. However the production in the metal walls of this species is not visible in the figure. The Fig. 4 (d) shows the constancy of the density of the $NO_2(X^2A_1)$ specie on the stream axis, after a sharp decrease, as shown by the 0D model. In contrast, the 2D simulation clearly shows the production of species in the larger section with increasing distance from the central axis of the flow. Ozone (Fig. 4 (e)) is formed regularly (increase of about 3 decades) from the end of discharge and leads to a relatively uniform distribution in the reactor. We denote the passage through a maximum before entering the large section of the reactor, which also predicted the 0D model. Again, we thus find a good consistency in results.

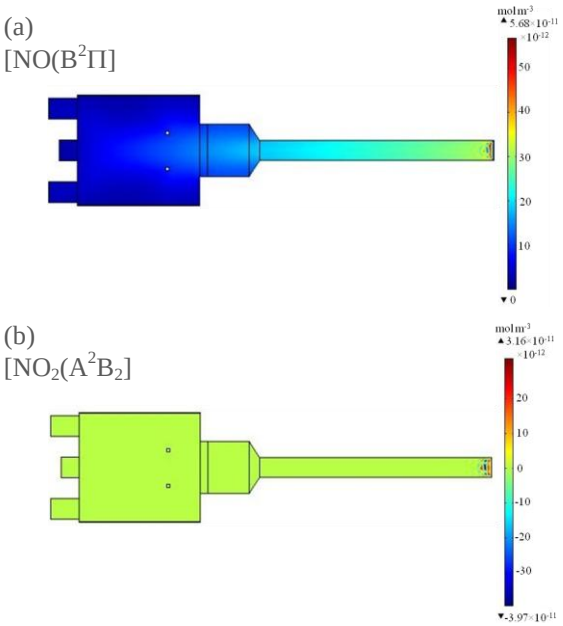

Fig. 5: Same simulation as in Fig. 4 but for NO and NO_2 species in excited states.

Concerning the $NO(B^2\Pi)$ state (Fig. 5 (a)) the results contrast with the ones on the fundamental state of the NO molecule (Fig. 4 (c)), showing strong dependence on the nitrogen atoms density. It is well outlooked by the similar density decrease from the end of the discharge (a factor of 3). The state $NO_2(A^2B_2)$ (Fig. 5 (b)) shows a substantially constant and very small distribution throughout the reactor. This results in consistence with the lack of detection of the signal by experiment and shown also by the 0D model.

5. Conclusion

The aim of this work was to present a successful combination of flow and kinetic modelling of N_2-O_2 late afterglows generated in a deposition reactor. We demonstrated that this kind of diagnostic coupled with experimental investigations can be a powerful tool for future studies to account notably for the main mechanisms and to simplify, to some extent, the possible reaction scheme. This is desired also on an industrial level to better predict the spatial distribution of active species and the nature of plasma processes like material treatment and thin film deposition without the use complex and full models.

Acknowledgement. This work was supported by the French Ministries of Foreign Affairs (MAE) and of Higher Education and Research (MESR) under the project 31802YA (PHC Stefanik 2014), by the Slovak Research and Development Agency under the project: SK-FR-2013-0035, by the Scientific Grant Agency of the Slovak Republic (VEGA) under the contract: 1/0925/14 and by Comenius University under the project: UK/491/2014. The authors would like to thank C. Malas for his technical help.

6. References

[1] S. Abou Rich, V. Mille, C. Vivien, S. Godey, P. Supiot, *Plasma Process. Polym.* **7** (2010) 775

[2] C. D. Pintassilgo, J. Loureiro, V. Guerra, *J. Phys. D: Appl. Phys.* **38** (2005), 417

[3] A. Ricard, O. Soo-ghee, V. Guerra, *Plasma Sources Sci. Technol.* **22** (2013) 035009

[4] A. Annušová, *Thèse*, Université Lille 1, France – Comenius University in Bratislava, Slovakia (2014)

[5] P. Mérel, M. Tabbal, M. Chaker, M. Moisan, A. Ricard, *Plasma Sources Sci. Technol.* **7** (1998) 550

[6] A. Annušová, C. Foissac, P. Veis, P. Supiot: submitted to *J. Phys. D: Appl. Phys.* (ref. JPhysD-104816) on 11th February, 2015